JOURNAL OF GUIDANCE, CONTROL, AND DYNAMICS
Vol. 34, No. 1, January–February 2011

Engineering Notes

Analytic Development of a Reference Trajectory for Skip Entry

Eduardo García-Llama*
GB Tech, Inc., Houston, Texas 77058

DOI: 10.2514/1.50798

I. Introduction

FOR entry vehicles with relatively low lift-to-drag ratios (L/D), a known strategy for achieving long downrange is to allow the vehicle to skip out of the atmosphere [1]. During this high-altitude and low-drag skip phase of the entry, the vehicle can dramatically increase its range. This Note is exclusively focused on entries from supercircular velocities that require an exoatmospheric phase to reach the landing site. Various methods have been suggested and implemented for atmospheric guidance of such trajectories. Most fall into one of three broad categories [2,3]: numeric predictor–correctors [4–9], analytic predictor–correctors [10,11], and reference-following controllers [12–16]. This Note presents a method, primarily intended for use under the latter category, that generates analytically a reference drag profile for the first entry portion of a skip entry when the exit conditions (and the initial conditions) are known. The analytic generation of such a reference profile has not been attempted before. In this way, this Note intends to contribute to the effort of developing a yet-unaccomplished complete analytic solution to the skip-entry guidance problem. Note that a complete analytic solution to the skip-entry problem should determine the conditions at exit (range to go, velocity V, and flight-path angle γ) that render the entry conditions for the final phase. The central difficulty in analytically determining the exit conditions lies in the limitations that various approximations and linearization assumptions have been found to have when estimating the range flown at low-drag altitudes [2,17–19]. The analytic determination of the exit conditions remains an elusive problem whose resolution is not intended in this Note.

The analytic development of a drag reference profile for a subcircular entry is the basis for the Space Shuttle Orbiter guidance logic [20]. This idea is based on the fact that the range to be flown during entry is a unique function of the drag acceleration maintained throughout the flight. This range is predictable using analytic techniques for simple geometric drag acceleration functions of the relative velocity (quadratic, linear, and constant, in the case of the orbiter), provided the local flight-path angle is small, which is the case at high speeds. Flight throughout the entry corridor can be achieved by linking these geometric functions together in a series. It is conceivable to divide the first entry in a skip trajectory in segments with linear and/or quadratic drag functions, as is the case in the space shuttle entry guidance; however, this approach will not be pursued in this Note. It is proposed in this Note to express the drag reference of the complete first entry as a polynomial function of the velocity, with degree *higher* than two. In addition, the generic method proposed to obtain the drag reference profile will be further simplified by thinking of the drag as the *probability density function* of the velocity or, conversely, by thinking of the velocity as the *distribution function* of the drag. With this notion, it will be shown that the reference drag profile can be generated by solving a system of linear algebraic equations.

For completeness, the drag profiles generated with this method will be tracked through the implementation of the feedback linearization method of differential geometric control as a guidance law with the error dynamics of a second-order homogeneous equation in the form of a damped oscillator [21]. Although this approach was first proposed as a revisited version of the Space Shuttle Orbiter entry guidance to demonstrate the commonality of both guidance laws, it has never been used to fly a skiplike entry trajectory, where the drag profile for the first entry does not fit a quadratic polynomial of the velocity.

A number of different approaches to skip-entry guidance for the Orion Crew Exploration Vehicle (CEV) spacecraft have been under evaluation at the Flight Mechanics and Trajectory Design Branch at NASA's Johnson Space Center [22]. A guidance algorithm called NSEG [19] (Numerical Skip Entry Guidance), which combines features of the original Apollo Guidance algorithm [23,24] with a numerical scheme for computing a real-time long-range skip trajectory, was found to provide very reliable means of meeting the skip-entry range requirement. Out of a comprehensive set of 60,000 skip-entry cases (20 nominal and 59,980 dispersed) that have been simulated for the CEV using NSEG, the 20 nominal cases will be used as test cases for this Note. As explained before, obtaining the skip-out exit conditions from the knowledge of the landing site and entry interface is not the objective of this Note; therefore, the initial and final conditions for testing purposes will be those pertaining to the 20 nominal trajectories. The 20 cases are subdivided into four groups. Each group is composed of five trajectories that have a common entry interface (EI in Fig. 1), but different target landing sites in the western continental United States and different L/D (0.3, 0.33, and 0.35).

II. Equations of Motion

The Earth-relative longitudinal translational state of the spacecraft is represented by the variables R (range), h (altitude above the Earth's surface), V (Earth-relative velocity), and γ (Earth-relative flight-path angle). The equations of motion in this document use a coordinate system with one axis oriented along the Earth-relative velocity vector, one axis perpendicular to the plane formed by the position and Earth-relative velocity vectors, and a third axis completing the right-hand coordinate system. The equations of motion are as follows:

$$\dot{R} = V\cos\gamma \tag{1}$$

$$\dot{h} = V\sin\gamma \tag{2}$$

$$\dot{V} = -D - g\sin\gamma \tag{3}$$

$$\dot{\gamma} = \frac{1}{V}\left[L\cos\phi + \left(\frac{V^2}{r_e + h} - g\right)\cos\gamma\right] \tag{4}$$

Presented as Paper 2007-6897 at the AIAA Atmospheric Flight Mechanics Conference and Exhibit, Hilton Head, SC, 20–23 August 2007; received 17 May 2010; revision received 10 September 2010; accepted for publication 18 September 2010.

*Contractor to NASA Johnson Space Center, Aeroscience and Flight Mechanics Division/EG5, 2101 Nasa Parkway. Professional Member AIAA.

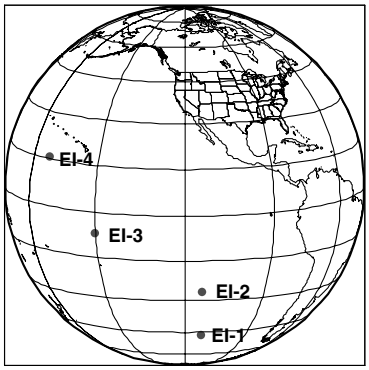

Fig. 1 Location of the test entry interfaces with respect to the United States.

where r_e is the mean Earth radius, g is the gravity acceleration, and ϕ is the bank angle. These equations of motion neglect the Coriolis and centripetal accelerations due to Earth's rotation because these accelerations are small compared to the aerodynamic acceleration.

The specific drag and lift are given by

$$D = \rho V^2 \left(\frac{S_r C_D}{2m} \right) \tag{5}$$

$$L = \rho V^2 \left(\frac{S_r C_L}{2m} \right) \tag{6}$$

where S_r and m are the reference surface and mass of the vehicle, respectively. The drag and lift aerodynamic coefficients (C_D and C_L) are assumed constant, since only hypersonic velocities are involved in the phase of interest.

An exponential atmospheric density model with constant atmospheric density at base altitude is assumed for this study:

$$\rho = \rho_0 e^{-\frac{h}{h_s}} \tag{7}$$

where h_s is the atmospheric density scale height.

III. Generation of the Reference Drag Profile

The phase under consideration is the first entry in a skip atmospheric entry. The origin for this phase is an initial velocity and flight-path angle, and the destination is a set of specific exit conditions in terms of velocity and flight-path angle at a desired range. A reference drag profile as a polynomial expression of the velocity is assumed:

$$D(V) = \sum_{n=0}^{m} a_n V^n \tag{8}$$

The $m + 1$ equations required to determine the coefficients a_n are then resolved. The problem is how to define the a_n coefficients. The solution is to find trajectory constraints that can be functionally related to the drag. There are five such basic constraints in all: four conditions on the initial and final (or exit) velocities and flight-path angles and a fifth condition on the range flown.

A. Defining the Basic Constraint Equations

Two equations relate the initial and final velocities to the initial and final drags:

$$D_{i,f} \equiv D(V_{i,f}) = \sum_{n=0}^{m} a_n V_{i,f}^n \tag{9}$$

where i and f refer to the initial and final (exit) states, respectively.

The relationship between the drag and the flight-path angle is derived using the equation for the atmospheric density. Differentiating Eq. (7) with respect to time produces the following equation:

$$\frac{\dot{\rho}}{\rho} = -\frac{\dot{h}}{h_s} \tag{10}$$

Differentiating Eq. (5) with respect to time, dividing by D, and combining with Eq. (10) results in

$$\frac{\dot{D}}{D} = -\frac{\dot{h}}{h_s} + \frac{2\dot{V}}{V} \tag{11}$$

Provided that $\dot{V} \approx -D$ for small flight-path angles, that $\dot{D} = \dot{V}\mathrm{d}D/\mathrm{d}V \approx -D\mathrm{d}D/\mathrm{d}V$, and that $\dot{h} = V \sin\gamma$, Eq. (11) results in

$$-\frac{\mathrm{d}D}{\mathrm{d}V} + \frac{2D}{V} = -\frac{V \sin\gamma}{h_s} \tag{12}$$

Hence, the other two equations relating the initial and final velocities and flight-path angles to the initial and final drags are

$$D'_{i,f} \equiv \left. \frac{\mathrm{d}D}{\mathrm{d}V} \right|_{i,f} = \frac{V_{i,f} \sin\gamma_{i,f}}{h_s} + \frac{2D_{i,f}}{V_{i,f}} = \sum_{n=0}^{m} n a_n V_{i,f}^{n-1} \tag{13}$$

A specific range R must be covered between the initial and final conditions. For small flight-path angles, combining Eqs. (1) and (3) and separating variables and integrating yields the equation on the range and thus the last of the five basic equations:

$$\begin{aligned} R &= -\int_{V_i}^{V_f} \frac{V}{D(V)}\,\mathrm{d}V = \int_{V_i}^{V_f} \frac{V}{\sum_{n=0}^{m} a_n V^n}\,\mathrm{d}V \\ &= \sum_{j=1}^{m} \frac{r_j}{\sum_{n=1}^{m} n a_n r_j^{n-1}} \log\left(\frac{V_i - r_j}{V_f - r_j} \right) \end{aligned} \tag{14}$$

where r_j are the roots of the polynomial $D(V)$. Having the drag expressed as a polynomial of the velocity implies that the integral in Eq. (14) can be solved analytically [25].

By solving the system composed of Eqs. (9), (13), and (14), a drag reference profile expressed as a degree 4 ($m = 4$) polynomial of the velocity can be generated. This system is composed of four linear equations (9) and (13) and one nonlinear equation (14). The form of the range equation (14) implies that numerical methods need to be used to find one of the coefficients in the drag polynomial from which the others could be derived analytically (see Appendix A). It would be highly desirable to find a relation such that the set of equations to obtain the coefficients of the drag polynomial could be solved as a linear system. The following development derives a replacement for Eq. (14) such that the system containing the five basic equations becomes a system of linear algebraic equations.

One way to achieve the desired linear equation is by relating the range to the integral of the drag along the velocity:

$$\int_{V_i}^{V_f} D(V)\,\mathrm{d}V = -\sum_{n=0}^{m} \frac{a_n}{n+1} (V_f^{n+1} - V_i^{n+1}) \tag{15}$$

However, in principle, it is only known how to relate range and drag through Eq. (14). The following steps are proposed to solve the integral in Eq. (15). Multiplying both sides of $\mathrm{d}V \approx -D\mathrm{d}t$ by the drag and integrating results in

$$\int_{V_i}^{V_f} D\,\mathrm{d}V = -\int_{t_i}^{t_f} D^2\,\mathrm{d}t \tag{16}$$

Expressing the integral on the right-hand side of Eq. (16) in terms of means and increments yields

$$\int_{V_i}^{V_f} D\,\mathrm{d}V = -\langle D^2 \rangle \Delta T \tag{17}$$

If a mean drag is associated with the phase under consideration, integrating Eq. (14) would result in $\langle D \rangle = (V_i^2 - V_f^2)/2R$. From the mean of the drag, the time duration of this phase can be found: $\Delta T = -\Delta V / \langle D \rangle$. To calculate the integral of interest, the mean of

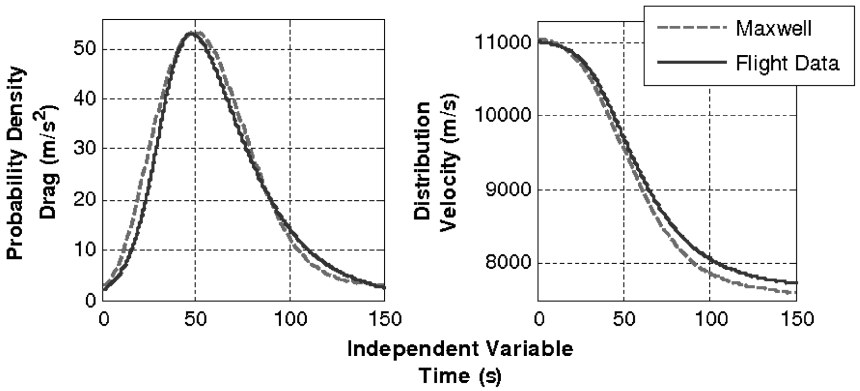

Fig. 2 Example of drag and velocity signals during the first entry in a skip entry compared to Maxwell probability density and distribution functions that have been properly scaled and initialized for comparison purposes.

the square of the drag must also be found. The next method is proposed to find $\langle D^2 \rangle$.

Note that a probability density function f is defined in terms of its distribution function F as $f(x) = \mathrm{d}F(x)/\mathrm{d}x$ [26]. The relation $\mathrm{d}V \approx -D\mathrm{d}t$ could be understood as the relation between a distribution function V and its probability density function D that have been specifically scaled and initialized. For instance, if it were not for the negative sign, the velocity *distribution* of the drag *probability density* would be very similar to the Maxwell distribution and density functions [26] (Fig. 2).

Assume that the drag in terms of time can be considered as a probability density function. In that case, $\langle D^2 \rangle$ and $\langle D \rangle^2$ are related through the variance, because the variance of a probability distribution is defined as $\sigma^2 = \langle x^2 \rangle - \langle x \rangle^2$. Provided that the variance in the Maxwell distribution is proportional to the square of the mean [26], it is reasonable to think that $\langle D^2 \rangle$ and $\langle D \rangle^2$ could ultimately be related through a linear function. From the 20 test cases referred to in the Introduction, the relationship between $\langle D^2 \rangle$ and $\langle D \rangle^2$ can be found empirically and checked if it follows a specific relation. Figure 3 presents that relation. A data correlation coefficient of 0.998 for the 20 nominal cases shows that $\langle D^2 \rangle$ and $\langle D \rangle^2$ are, in fact, highly correlated (this analysis was also carried out for the 59,980 dispersed cases. For the dispersed cases, the correlation coefficient was found to be 0.985).

From Fig. 3 it is deduced that

$$\langle D^2 \rangle = k_{d1} \langle D \rangle^2 + k_{d2} \tag{18}$$

where k_{d1} and k_{d2} are the regression constants. The range equation (14) can now be substituted with

$$\sum_{n=0}^{m} \frac{a_n}{n+1} (V_f^{n+1} - V_i^{n+1}) = (k_{d1} \langle D \rangle^2 + k_{d2}) \Delta T \tag{19}$$

which could be considered a pseudorange equation, because the range is indirectly accounted for through the terms $\langle D \rangle$ and ΔT.

B. Additional Constraint Equation

Should it be desired to add constraint equations to the drag profile, the degree of the drag polynomial should be increased accordingly. In this section, one additional constraint equation will be generated. From the equations derived so far, the drag reference profile may turn out to have a maximum drag acceleration at an arbitrary velocity ($V_{D_{\max}}$). It is desired to generate drag reference profiles whose shapes are more in line with realistic shapes. From the cases simulated with NSEG, a quite simple trend can be found by inspection of the drag profiles: the velocity at which the maximum drag occurs has a high correlation with the product of the initial and final velocities (Fig. 4). The correlation factor was found to be 0.991 for the 20 nominal test cases (for the 59,980 dispersed cases the correlation coefficient was found to be 0.851).

Therefore, the additional constraint equation will be given by

$$D'_{D_{\max}} = \sum_{n=0}^{m} n a_n V_{D_{\max}}^{n-1} = 0 \tag{20}$$

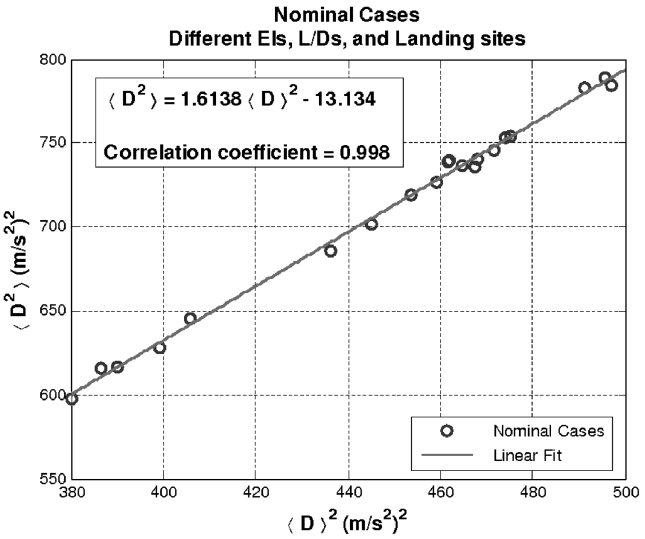

Fig. 3 Relation between $\langle D^2 \rangle$ and $\langle D \rangle^2$ in the phase of interest for the 20 nominal skip entries flown using NSEG.

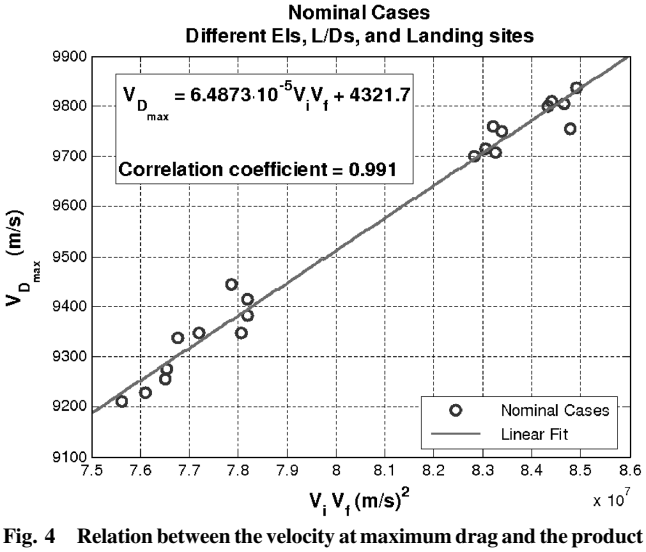

Fig. 4 Relation between the velocity at maximum drag and the product of the initial and final velocities in the phase of interest for the 20 nominal skip entries flown using NSEG.

where the velocity at maximum drag, $V_{D_{\max}}$, can be expressed as

$$V_{D_{\max}} = k_{v1} V_i V_f + k_{v2} \tag{21}$$

where k_{v1} and k_{v2} are the regression constants.

C. General Solution to Generate Drag Reference Profiles

From the results obtained in the previous subsections, the system of five or six linear equations (depending on whether the drag is expressed as a 4 or 5 deg polynomial, respectively) from where the reference drag profiles can be obtained is

$$\begin{pmatrix} 1 & V_i & V_i^2 & V_i^3 & V_i^4 & | & V_i^5 \\ 1 & V_f & V_f^2 & V_f^3 & V_f^4 & | & V_f^5 \\ 0 & 1 & 2V_i & 3V_i^2 & 4V_i^3 & | & 5V_i^4 \\ 0 & 1 & 2V_f & 3V_f^2 & 4V_f^3 & | & 5V_f^4 \\ \frac{V_f - V_i}{1} & \frac{V_f^2 - V_i^2}{2} & \frac{V_f^3 - V_i^3}{3} & \frac{V_f^4 - V_i^4}{4} & \frac{V_f^5 - V_i^5}{5} & | & \frac{V_f^6 - V_i^6}{6} \\ --- & --- & --- & --- & --- & | & --- \\ 0 & 1 & 2V_{D_{\max}} & 3V_{D_{\max}}^2 & 4V_{D_{\max}}^3 & | & 5V_{D_{\max}}^4 \end{pmatrix} \times \begin{pmatrix} a_0 \\ a_1 \\ a_2 \\ a_3 \\ a_4 \\ -- \\ a_5 \end{pmatrix} = \begin{pmatrix} D_i \\ D_f \\ \frac{V_i \sin\gamma_i}{h_s} + \frac{2D_i}{V_i} \\ \frac{V_f \sin\gamma_f}{h_s} + \frac{2D_f}{V_f} \\ \langle D^2 \rangle \Delta T \\ ------ \\ 0 \end{pmatrix} \tag{22}$$

Figure 5 shows the degree 5 and degree 4 drag reference profiles generated using Eq. (22) when the range and the initial and final conditions of the 20 nominal test cases are used. With generality, a skip entry is defined whenever the lofting acceleration drops below 0.2 g during the lofting phase of the flight. Therefore, for the generation of the profiles, the final drag and, for simplicity, the initial drag are chosen to be 0.2 g. For comparison, the nominal ranges covered during the first entry in the 20 nominal cases flown using NSEG are shown in Fig. 6.

D. Feasibility of the Generated Drag Profiles

Given a reference profile $D(V)$, can the existence of a feasible bank control command be guaranteed such that $D(V)$ can be tracked? The approach to derive the reference bank control consists of time differentiating the drag along the trajectory (i.e., taking the Lie derivative of the drag) until the first appearance of the control. This has been done in [20,21], where the reference bank angle was found to be

$$\phi = \arccos\left\{\left(\ddot{D} - \dot{D}\left(\frac{\dot{D}}{D} - \frac{3D}{V}\right) + \frac{4D^3}{V^2} + \frac{D}{\langle h_s \rangle}\left(\frac{V^2}{r_e + \langle h \rangle} - \langle g \rangle\right)\right)\left(\frac{-D^2}{(L/D)\langle h_s \rangle}\right)^{-1}\right\} \tag{23}$$

where the mean values of g, h_s, and h have been used. To find the second time derivative of the drag to be substituted in Eq. (23), it is necessary to differentiate the equation $\dot{D} \approx -D\mathrm{d}D/\mathrm{d}V$ a second time. This operation results in

$$\ddot{D} = D\left(\frac{\mathrm{d}D}{\mathrm{d}V}\right)^2 + D^2 \frac{\mathrm{d}^2 D}{\mathrm{d}V^2} \tag{24}$$

The resulting bank-angle profiles, corresponding to the fifth- and fourth-order drag reference profiles depicted in Fig. 5, are shown in Fig. 7. A saturation at 180° exists at the beginning of the trajectories (high velocities) for a small velocity interval, when the drag is still fairly low. The following section will show how this feature is dealt with when the control law is implemented. Except for this undesired trait, the bank-angle profiles remain completely feasible.

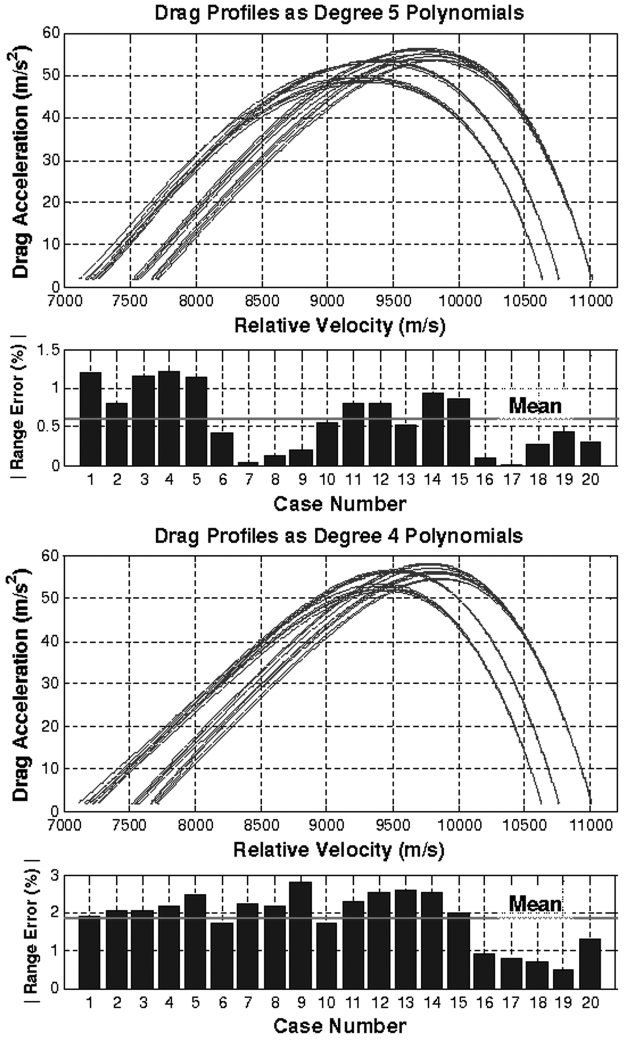

Fig. 5 Drag reference profiles generated using Eq. (22) and resulting range errors with respect to the ranges of the 20 nominal skip-entry cases flown using NSEG.

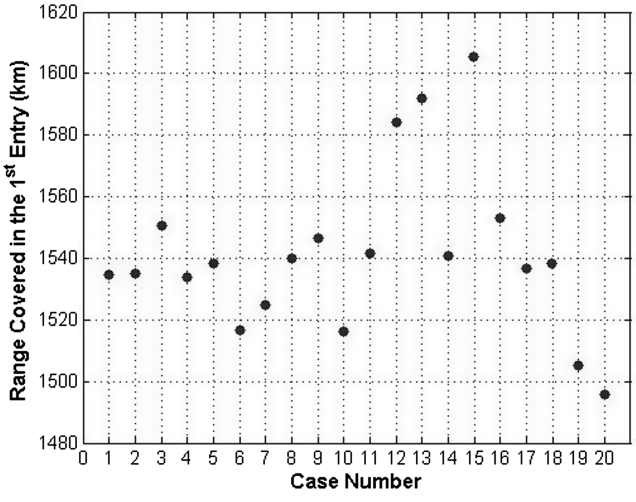

Fig. 6 Ranges covered during the first entry in the 20 nominal cases flown using NSEG.

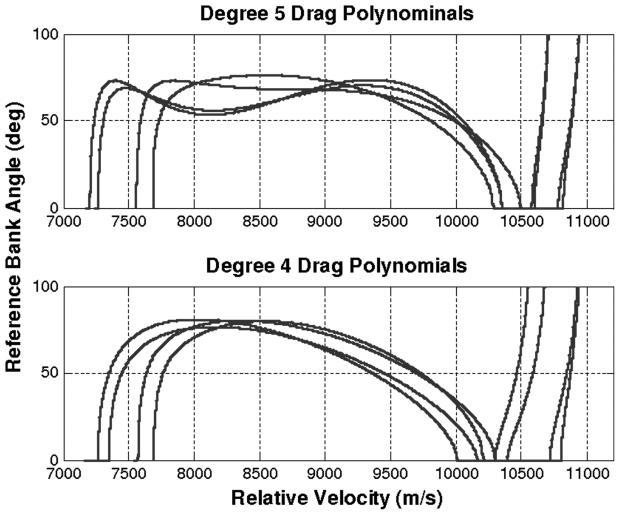

Fig. 7 Reference bank-angle profiles associated with the fifth-order drag reference profiles generated using Eq. (22).

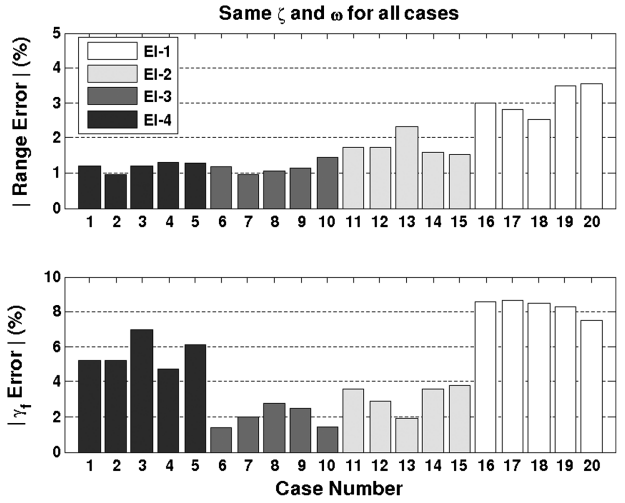

Fig. 8 Absolute range and final flight-path-angle errors of the controlled trajectories with respect to the values of the 20 nominal skip-entry cases flown using NSEG.

IV. Reference Profile Tracking

For completeness, a bank-angle control law will be implemented for tracking the reference profiles. The control law is based on the guidance law for the Space Shuttle Orbiter revisited using nonlinear geometric methods, with the error dynamics of a second-order homogeneous equation in the form of a damped oscillator. This work is detailed in [21], and therefore its theoretical development and background will not be presented here.

The control law presented in [21] guarantees perfect tracking of either a drag in the form of a linear function of the velocity or a quadratic drag with a constant error in steady state, because it accounts for two integrators in the plant. The generated reference drag profiles (Fig. 5), although polynomials of the velocity of degree 4 or 5, at low velocities approximate a linear function of the velocity, which can be tracked with zero steady-state error with a double integrator. The performance remains to be seen of such a controller at high velocities, where the drag profile does not have a linear behavior. This section will show that satisfactory performance is achieved using the double-integrator control scheme.

The translational state is controlled by adjusting the vertical lift-to-drag ratio, $(L/D)\cos\phi$. Equivalently, the bank angle ϕ is taken to be the control in the following analysis. The control law derived in [21] is given by

$$\phi_c = \arccos\left\{\frac{1}{(L/D)b_r}(-a_r + \ddot{D}_r - \omega^2\Delta D - 2\zeta\omega\Delta\dot{D})\right\} \quad (25)$$

where the subindex r refers to the reference profile and where ω and ζ are the natural frequency and the damping ratio, respectively. The terms a_r and b_r are given by

$$a_r = \dot{D}_r\left(\frac{\dot{D}_r}{D_r} - \frac{3D_r}{V}\right) - \frac{4D_r^3}{V^2} + \left(\langle g\rangle - \frac{V^2}{r_e + \langle h\rangle}\right)\frac{D_r}{\langle h_s\rangle} \quad (26)$$
$$b_r = -D_r^2/\langle h_s\rangle$$

The performance of the drag tracking control is evaluated on the 20 drag profiles with degree 5 shown in Fig. 5. The same set of control gains is used for all the cases, regardless of the initial and final conditions. During the controlled simulation, the drag profile is not updated or modified to reduce the range error. Therefore, the target miss accumulated at guidance termination will be a measure of the control performance.

In all simulations, the control starts operating once the initial drag acceleration is higher than 1 g. Before that point, the commanded bank angle is constant and equal to 80 deg to avoid the saturation observed in the reference bank angle at the initiation of the entry (Fig. 7). The bank-angle rate of change and acceleration were limited to $\pm 15\,\mathrm{deg/s}$ and $\pm 6\,\mathrm{deg/s^2}$, respectively. Each controlled simulation is divided in two phases, determined by the velocity and the curvature of the drag as a function of the velocity. Figure 5 shows that the drag reference profiles become almost linear at low velocities. It was determined that changing the set of control gains when the curvature was smaller than a certain threshold resulted in an improvement of the tracking performance. The curvature is defined as $\kappa = (\mathrm{d}^2D/\mathrm{d}V^2)/(1 + (\mathrm{d}D/\mathrm{d}V)^2)^{3/2}$, [27] and its threshold was chosen to be -0.05. The selected values of the control gains in phase 1 (high velocities) are $\zeta = 0.4$ and $\omega = 3/(80\zeta) = 0.0938$. In

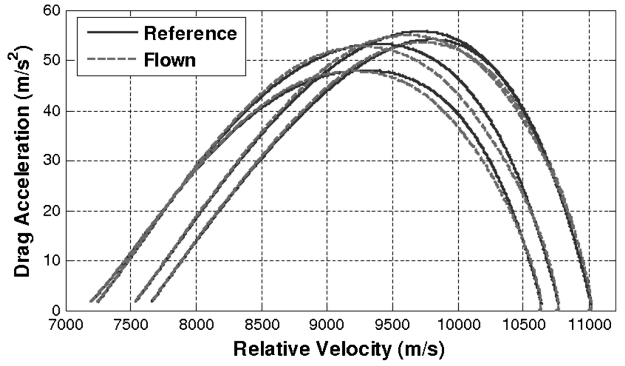

Fig. 9 Examples of drag-vs-velocity profiles of four controlled trajectories, one from each entry interface.

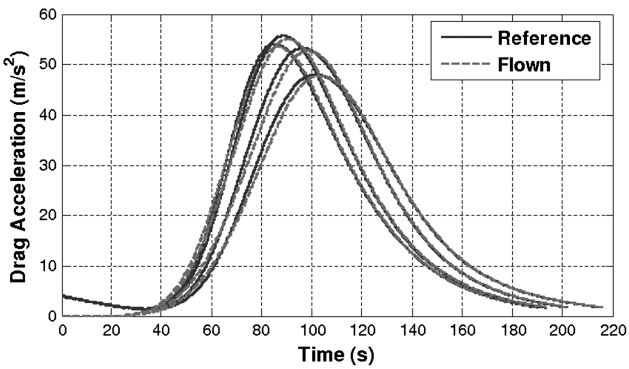

Fig. 10 Examples of drag-vs-time profiles of four controlled trajectories, one from each entry interface.

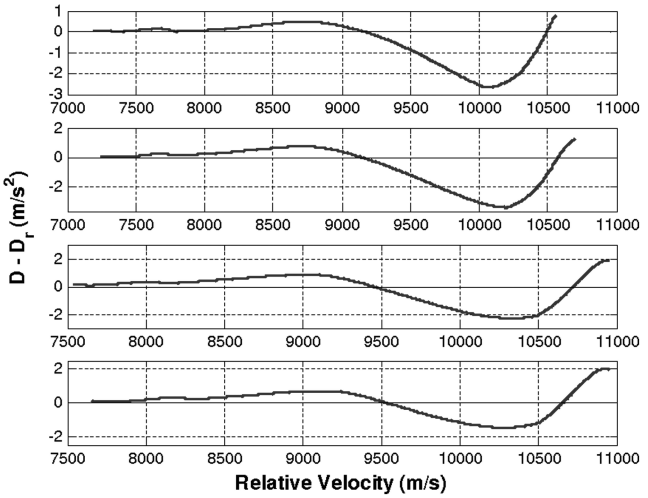

Fig. 11 Examples of drag acceleration error signals of four controlled trajectories, one from each entry interface.

phase 2 (low velocities and $-0.05 < \kappa < 0$) the control gains are $\zeta = 0.68$ and $\omega = 3/(25\zeta) = 0.1765$. Note that the 5% criteria [28] (settling time equal to three times the time constant of the system) has been used for the calculation of ω.

Figure 8 shows, for each of the test cases, the absolute range and final flight-path angle percentile errors with respect to the values in the 20 nominal cases flown using NSEG. Figure 8 depicts similar error values for the cases with the same entry interface. This suggests that specific sets of control gains could be selected for each group with the same entry interface to improve the tracking performance. Furthermore, the latter could imply that an optimal relation between control gains and the set of initial and final conditions could be found. Nevertheless, this possibility is not explored here, because it is not the objective of this Note to develop the control law to fly the drag profiles. Eventually, the control law could be as sophisticated as desired.

Figures 9 and 10 show the results of four controlled trajectories, one from each entry interface. Figure 11 shows the drag error signals for the same set of four trajectories.

V. Conclusions

This Note shows that a feasible reference drag profile for the first entry portion of a skip entry can be generated as a polynomial expression of the velocity. The coefficients of that polynomial are found through the resolution of a system composed of $m + 1$ equations, where m is the degree of the drag polynomial. It has been shown that a minimum of five equations ($m = 4$) are required to establish the range and the initial and final conditions on velocity and flight-path angle. It has been shown that at least one constraint on the trajectory can be imposed through the addition of one extra equation in the system, which must be accompanied by the increase in the degree of the drag polynomial.

To simplify the resolution of the system of equations, the drag was considered as being a probability density function of the velocity, with the velocity as a distribution function of the drag. Combining this notion with the introduction of empirically derived constants, it has been shown that the system of equations required to generate the drag profile can be successfully reduced to a system of linear algebraic equations.

For completeness, the resulting drag profiles have been flown using the feedback linearization method of differential geometric control as a guidance law with the error dynamics of a second-order homogeneous equation in the form of a damped oscillator. Satisfactory results were achieved when the gains in the error dynamics were changed at a certain point along the trajectory that is dependent on the velocity and the curvature of the drag as a function of the velocity.

Appendix A: Reference Profile Calculation Using the Range Equation

When the five basic equations are used to generate a drag reference profile, the drag polynomial must have degree 4 ($m = 4$) to result in five unknown coefficients $(a_0, \ldots, a_4)$. The range equation (14) implies that numerical methods need to be used to find at least one of the coefficients in the drag polynomial from which the others can be derived analytically. For example, if a_3 is the coefficient selected, a_0, a_1, a_2, and a_4 will be expressed in terms of a_3.

To simplify the expressions, the following definition is made:

$$\Delta^{(n)}V \equiv V_f^n - V_i^n, \qquad n > 1 \tag{27}$$

The system of four linear equations (range equation not included) is given by

$$\begin{pmatrix} 1 & V_i & V_i^2 & V_i^3 & V_i^4 \\ 1 & V_f & V_f^2 & V_f^3 & V_f^4 \\ 0 & 1 & 2V_i & 3V_i^2 & 4V_i^3 \\ 0 & 1 & 2V_f & 3V_f^2 & 4V_f^3 \end{pmatrix} \begin{pmatrix} a_0 \\ a_1 \\ a_2 \\ a_3 \\ a_4 \end{pmatrix} = \begin{pmatrix} D_i \\ D_f \\ D_i' \\ D_f' \end{pmatrix} \tag{28}$$

A symbolic Gaussian elimination in Eq. (28) results in the following equations for the coefficients a_0, a_1, a_2, and a_4 expressed in terms of a_3:

$$\begin{gathered} a_4 = b_{4_1} + b_{4_2}a_3 \qquad a_2 = b_{2_1} + b_{2_2}a_3 \qquad a_1 = b_{1_1} + b_{1_2}a_3 \\ a_0 = b_{0_1} + b_{0_2}a_3 \end{gathered} \tag{29}$$

where

$$\begin{aligned} b_{4_1} &= (\Delta D'(2V_i - \Delta^{(2)}V/\Delta V) + 2\Delta D - 2D_i'\Delta V)/k \\ b_{4_2} &= -(3\Delta^{(2)}V(2V_i - \Delta^{(2)}V/\Delta V) - 2(3V_i^2\Delta V - \Delta^{(3)}V))/k \\ k &= 4\Delta^{(3)}V(2V_i - \Delta^{(2)}V/\Delta V) - 2(4V_i^3\Delta V - \Delta^{(4)}V) \\ b_{2_1} &= (\Delta D' - 4b_{4_1}\Delta^{(3)}V)/(2\Delta V) \\ b_{2_2} &= -(3\Delta^{(2)}V + 4b_{4_2}\Delta^{(3)}V)/(2\Delta V) \\ b_{1_1} &= (\Delta D - b_{2_1}\Delta^{(2)}V - b_{4_1}\Delta^{(4)}V)/\Delta V \\ b_{1_2} &= -(b_{2_2}\Delta^{(2)}V + \Delta^{(3)}V + b_{4_2}\Delta^{(4)}V)/\Delta V \\ b_{0_1} &= D_i - b_{1_1}V_i - b_{2_1}V_i^2 - b_{4_1}V_i^4 \\ b_{0_2} &= -(b_{1_2}V_i + b_{2_2}V_i^2 + V_i^3 + b_{4_2}V_i^4) \end{aligned} \tag{30}$$

Note that the roots of a quartic polynomial can be found analytically [25]. Thus, the roots of the drag polynomial r_j in Eq. (14)

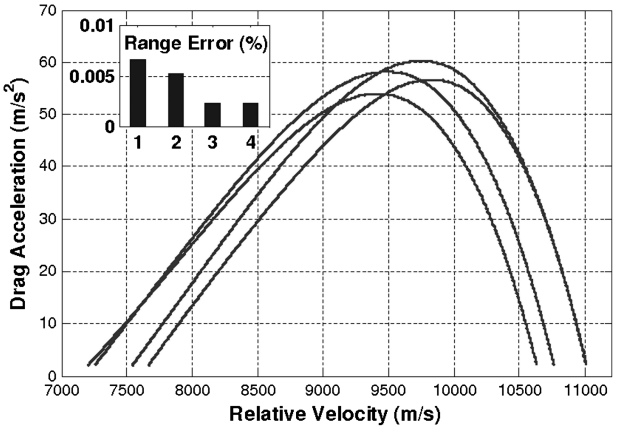

Fig. A1 Four drag reference profiles, one from each entry interface, generated using the range equation (14), and resulting absolute range errors with respect to the actual ranges of the corresponding test nominal skip-entry cases flown using NSEG.

can be expressed as $r_j = r_j(a_0, \ldots, a_4)$, which implies that $r_j = r_j(a_3)$ in the case derived here. Hence, with these results, the problem has been reduced to numerically finding the coefficient a_3 that satisfies the range equation (14), which, in this particular case, can be written as follows:

$$R = \sum_{j=1}^{4} \frac{r_j(a_3)}{\sum_{n=1}^{4} n a_n(a_3)(r_j(a_3))^{n-1}} \log\left(\frac{V_i - r_j(a_3)}{V_f - r_j(a_3)}\right) \tag{31}$$

Using this method, drag reference profiles were generated for four of the 20 nominal cases considered in this study, one for each entry interface. Those profiles are depicted in Fig. A1.

Acknowledgments

The author wants to thank the following people at the Flight Mechanics and Trajectory Design Branch at NASA's Johnson Space Center: Christopher J. Cerimele and Lee E. Bryant, respectively, Branch Chief and Deputy Chief; Jeremy R. Rea of the Orion Crew Exploration Vehicle Entry Guidance team; and Juan S. Senent, Odyssey Space Research LLC contractor.

References

[1] Eggers, A. J., Jr., Allen, H. J., and Niece, S. E., "A Comparative Analysis of the Performance of Long-Range Hypervelocity Vehicles," Ames Aeronautical Lab., NACA TR 1382, Moffett Field, CA, 1958.

[2] Bairstow, S. H., "Reentry Guidance with Extended Range Capability for Low L/D Spacecraft," S.M. Thesis, Dept. of Aeronautics and Astronautics, Massachusetts Inst. of Technology, Cambridge, MA, Feb. 2006.

[3] Wingrove, R. C., "Survey of Atmosphere Re-Entry Guidance and Control Methods," *AIAA Journal*, Vol. 1, No. 9, Sept. 1963, pp. 2019–2029.
doi:10.2514/3.1987

[4] Bryant, J. P., and Frank, M. P., "Supercircular Reentry Guidance for a Fixed L/D Vehicle Employing a Skip for Extreme Ranges," American Rocket Society, Paper 2489-62, July 1962.

[5] Powell, R. W., "Numerical Roll Reversal Predictor Corrector Aerocapture and Precision Landing Guidance Algorithms for the Mars Surveyor Program 2001 Missions," AIAA Atmospheric Flight Mechanics Conference and Exhibit, Boston, MA, AIAA Paper 1998-4574, Aug. 1998.

[6] Youssef, H., Chowdhry, R., Lee, H., Rodi, P., and Zimmerman, C., "Predictor-Corrector Entry Guidance for Reusable Launch Vehicles," AIAA Guidance, Navigation, and Control Conference and Exhibit, Montreal, AIAA Paper 2001-4043, Aug. 2001.

[7] Bairstow, S. H., and Barton, G. H., "Orion Reentry Guidance with Extended Range Capability Using PredGuid," AIAA Guidance, Navigation and Control Conference and Exhibit, Hilton Head, SC, AIAA Paper 2007-6427Aug. 2007.

[8] Lu, P., "Predictor-Corrector Entry Guidance for Low-Lifting Vehicles," *Journal of Guidance, Control, and Dynamics*, Vol. 31, No. 4, July–Aug. 2008, pp. 1067–1075.

[9] Brunner, C. W., and Lu, P., "Skip Entry Trajectory Planning and Guidance," *Journal of Guidance, Control, and Dynamics*, Vol. 31, No. 5, Sept.–Oct. 2008, pp. 1210–1219.
doi:10.2514/1.35055

[10] Chapman, P. W., and Moonan, P. J., "Analysis and Evaluation of a Proposed Method for Inertial Reentry Guidance of a Deep Space Vehicle," *Proceedings of the National Aerospace Electronics Conference*, Dayton, OH, May 1962, pp. 579–586.

[11] Mease, K., and McCreary, F., "Atmospheric Guidance Law for Planar Skip Trajectories," 12th Atmospheric Flight Mechanics Conference, Snowmass, CO, AIAA Paper 1985-1818Aug. 1985.

[12] Wingroue, R. C., "A study of Guidance to Reference Trajectories for Lifting Reentry at Supercircular Velocity," NASA Ames Research Center, TN D-2818, Moffett Field, CA, May 1965.

[13] Coate, R. E., Lessing, H. C., and Tunnel, P. J., "Lunar Landing and Long-Range Earth Re-Entry Guidance by Application of Perturbation Theory," *Journal of Spacecraft and Rockets*, Vol. 1, No. 2, 1964, pp. 191–196.
doi:10.2514/3.27621

[14] Lessing, H. C., and Coate, R. E., "Guidance of a Low L/D Vehicle Entering the Earth's Atmosphere at Speeds up to 50,000 Feet Per Second," NASA Ames Research Center, TN D-2818, Moffett Field, CA, May 1965.

[15] Morth, R., "Reentry Guidance for Apollo," MIT/IL R-532, Vol. 1, Jan. 1966.

[16] Gilbert, L. C., and Dallas, G. I., "Apollo-Derived Mars Precision Lander Guidance," AIAA Atmospheric Flight Mechanics Conference and Exhibit, Boston, MA, AIAA Paper 1998-4570Aug. 1998.

[17] Naidu, D., "Three-Dimensional Atmospheric Entry Problem Using Method of Matched Asymptotic Expansions," *IEEE Transactions on Aerospace and Electronic Systems*, Vol. 25, No. 5, Sept. 1989, pp. 660–667.
doi:10.1109/7.42083

[18] Kuo, Z., and Vinh, N., "Improved Matched Asymptotic Solutions for Three-Dimensional Atmospheric Skip Trajectories," *Journal of Spacecraft and Rockets*, Vol. 34, No. 4, 1997, pp. 496–502.
doi:10.2514/2.3239

[19] Tigges, M., Crull, T., Rea, J., and Johnson, W., "Numerical Skip-Entry Guidance," Guidance and Control Conference, Breckenridge, CO, American Astronautical Society, Paper 07-076, Feb. 2007.

[20] Harpold, J. C., and Graves, C. A., "Shuttle Entry Guidance," *Journal of the Astronautical Sciences*, Vol. 27, No. 3, 1979, pp. 239–268.

[21] Mease, K. D., and Kremer, J-P., "Shuttle Entry Guidance Revisited Using Nonlinear Geometric Methods," *Journal of Guidance, Control, and Dynamics*, Vol. 17, No. 6, Nov.–Dec. 1994, pp. 1350–1356.
doi:10.2514/3.21355

[22] Rea, J., and Putnam, Z., "A Comparison of Two Orion Skip Entry Guidance Algorithms," AIAA Guidance, Navigation and Control Conference and Exhibit. Hilton Head, SC, AIAA Paper 2007-6424, Aug. 2007.

[23] Moseley, P. E., "The Apollo Entry Guidance: A Review of the Mathematical Development and Its Operational Characteristics," TRW Rept. 69-FMT-791, 1 Dec. 1969.

[24] Graves, C. A., and Harpold, J. C., "Apollo Experience Report. Mission Planning for Apollo Entry," NASA Manned Spacecraft Center TN D-6725, Houston, TX, March 1972.

[25] Zwillinger, D., *Mathematical Tables and Formulae*, 30th ed., CRC Press, Boca Raton, FL, 1996, p. 83.

[26] Papoulis, A., *Probability, Random Variables, and Stochastic Processes*, 3rd ed., McGraw–Hill, New York, 1991.

[27] Kobayashi, S., and Nomizu, K., *Foundations of Differential Geometry*, Wiley-Interscience, New York, 1996.

[28] Ogata, K., *Modern Control Engineering*, 5th ed., Prentice–Hall, New York, 2009.